Dynamical and sequential decay effects on isoscaling and density dependence of the symmetry energy

W. D. Tian[1*], Y. G. Ma[1†], X. Z. Cai[1], D. Q. Fang[1], W. Guo[1,2], C. W. Ma[1,2], G. H. Liu[1,2], W. Q. Shen[1], Y. Shi[1,2], H. W. Wang[1], K. Wang[1,2], W. Xu[1], T. Z. Yan[1,2]

1) Shanghai Institute of Applied Physics, Chinese Academy of Sciences, P. O. Box 800-204, Shanghai 201800, China

2) Graduate School of Chinese Academy of Sciences, Beijing, 100049, China

(Dated: February 9, 2008)

The isoscaling properties of the primary and final products are studied via isospin dependent quantum molecular dynamics (IQMD) model and the followed sequential decay model GEMINI, respectively. It is found that the isoscaling parameters α of both primary and final products keep no significant change for light fragments, but increases with the mass for intermediate and heavy products. The dynamical effects on isoscaling are exhibited by that α value decreases a little with the evolution time of the system, and opposite trend for the heavy products. The secondary decay effects on isoscaling are reflected in the increasing of the α value for the final products which experiences secondary decay process. Furthermore the density dependence of the symmetry energy has also been explored, it is observed that in the low densities the symmetry energy coefficient has the form of $C_{sym}(\rho) \sim C_0(\rho/\rho_0)^\gamma$, where $\gamma = 0.7 \sim 1.3$ for both primary and final products, but C_0 have different values for primary and final products. It is also suggested that it might be more reasonable to describe the density dependence of the symmetry energy coefficient by the $C_{sym}(\rho/\rho_0) \approx C_1(\rho/\rho_0)^{\gamma_{soft}} + C_2(\rho/\rho_0)^{\gamma_{stiff}}$ with $\gamma_{soft} \leq 1$, $\gamma_{stiff} \geq 1$ and C_1, C_2 constant parameters.

PACS numbers: 24.10.Nz, 24.10.-i, 25.70.Pq, 25.70.-z, 24.80.+y

I. INTRODUCTION

The isotopic composition of the nuclear reaction products [1] contains important information on the role of the isospin on the reaction process. Recently increased interest in the N/Z degree of freedom and its equilibration, as well as the isospin asymmetry dependent terms of the nuclear equation of state (EOS) [2, 3, 4, 5, 6, 7], has motivated detailed measurements of the isotopic distributions of reaction products. It has been shown that isospin effects can be studied by comparing the yields of fragments from two similar reactions that differ only in the isospin asymmetry [8, 9], in this case, the effect of sequential decay of primary fragments can be bypassed to a large extent. It has been revealed that for statistical fragment production mechanism(s), if two reactions occurring at the similar temperature have different isospin asymmetry, the ratio $R_{21}(N, Z)$ of the yields of a given fragment N and Z obtained from the two reactions 2 and 1 exhibits an exponential dependence on N and Z of the form [9, 10, 11]

$$R_{21}(N, Z) = Y_2(N, Z)/Y_1(N, Z) = C \exp(\alpha N + \beta Z), \quad (1)$$

where α and β are two scaling parameters and C is an overall normalization constant. This behavior is called isoscaling [10]. Isoscaling has been obtained in different reactions and theoretical calculations, such as in evaporation reactions [12], deep inelastic reactions [13, 15], fission

reactions [14] and multifragmentations [8, 9, 16, 17, 18], where is the biggest amount of experimental isoscaling data comes from. Isoscaling phenomena in different reaction mechanisms have also been investigated by various theoretical models, such as Langevin equation combining with the statistical decay model for the fission dynamics [19, 20], isospin-dependent Lattice Gas model [21] for the multifragmentations, Anti-symmetrized Molecular Dynamics (AMD) model [22], Isospin dependent Quantum Molecular Dynamics model [23], Microcanonical Statistical Multifragmentation model, Expanding Emitting Source model, Canonical model [11], Microcanonical Multifragmentation model [24] and so on.

The isospin dependence of the nuclear equation of state (EOS) is one of the most important properties in nuclear matter and reactions, in particular in nuclear astrophysics, supernova and neutron stars [1, 25]. Although the nuclear symmetry energy at normal nuclear matter density $\rho_0 = 0.16 fm^{-3}$ has been determined to be around 30 MeV from the empirical liquid-drop mass formula [26], however, its values at sub- and super-densities are poorly known. Studies based on various theoretical models also give widely different predictions [1, 18, 27, 28]. Multifragmentation is generally considered as a low density phenomenon with a high degree of thermalization which is believed to be reached. It has been shown [11, 16] that the isoscaling parameter α is directly related to the coefficient C_{sym} of the symmetry energy term of the nuclear binding energy, the following relation has been obtained both in the framework of the grand-canonical limit of the statistical multifragmentation model [11] and in the expanding-emitting source

model [16]:

$$\alpha = 4\frac{C_{sym}}{T}\left[\left(\frac{Z_1}{A_1}\right)^2 - \left(\frac{Z_2}{A_2}\right)^2\right] \qquad (2)$$

where Z_1, A_1, and Z_2, A_2 refer to the charge number and mass number of the fragments from reactions 1 and 2 respectively. Using this relation, from the extracted values of α and T of the fragments in the reaction, symmetry energy coefficient C_{sym} in the EOS could be derived.

The paper aims to investigate isoscaling in multifragmentation reactions by the dynamical IQMD model and the afterburner sequential decay model GEMINI calculation, explore the dynamical and secondary decay effects on the isoscaling phenomenon. Different isoscaling properties between light and heavy products have revealed. Through the relationship of equation (2) between isoscaling parameter α and symmetry energy coefficient C_{sym}, the form of symmetry energy density dependence can be deduced. Section II gives a brief review of the IQMD and GEMINI model. Section III presents the IQMD and IQMD+GEMINI calculation results on isoscaling obtained from the different system evolution time, primary and final products, discusses the properties of the isoscaling parameter α. Section IV investigates the density dependence of the symmetry energy coefficient C_{sym} for the primary and final products following some results in section III. The conclusions are drawn in section V.

II. MODEL OVERVIEW

A. Dynamical model: IQMD

The Quantum Molecular Dynamics (QMD) model approach is an n-body theory to describe heavy ion reactions from intermediate energy to several GeV/nucleon, it is classical in essence because the time evolution of the system is determined by classical canonical equation of motion, however many important quantum features are included in this prescription. At intermediate energies the heavy ion collision is mainly governed by three components: the mean field, two-body collision and Pauli blocking. General review about the QMD can be found in reference of Aichelin [29] together with several other similar models such as AMD [31] and Constrained Molecular Dynamics (CoMD) model [32].

The IQMD model is based on the general QMD to include explicitly isospin-degrees of freedom [30]. In the QMD model, each nucleon is represented by a Gaussian wave packet,

$$\psi_i(\mathbf{r}, \mathbf{p}) = \frac{1}{(2\pi L)^{3/4}} \exp\left[-\frac{(\mathbf{r} - \mathbf{r}_i)^2}{4L} + i\mathbf{r} \cdot \mathbf{p}\right] \qquad (3)$$

where $\mathbf{r_i}$ is the center of the ith wave packet in the coordinate space, and L is the so-called Gaussian wave packet width (here $L = 2.16 fm^2$). The total N-body wave function is assumed to be the direct product of these coherent

states. Through a Wigner transformation of the wave function, defining $L = \sigma_r^2$ and $\sigma_p^2 = \hbar^2/4\sigma_r^2 = \hbar^2/4L$ the N-body phase-space distribution function is given by a symmetry form in coordinate and momentum space

$$f(\mathbf{r}, \mathbf{p}) = \sum_i \frac{1}{(\pi\hbar)^3} \exp\left[-\frac{(\mathbf{r} - \mathbf{r}_i)^2}{2\sigma_r^2} - \frac{(\mathbf{p} - \mathbf{p}_i)^2}{2\sigma_p^2}\right], \quad (4)$$

here $\mathbf{r_i}$ and $\mathbf{p_i}$ are the center of the ith wave packet in the coordinate and momentum space, σ_r and σ_p are the widths of wave packets in coordinate and momentum space, respectively. The Wigner representation of the Gaussian wave packet obeys the uncertainty relation $\sigma_r\sigma_p = \hbar/2$. The densities in coordinate and in momentum space are given by

$$\rho(\mathbf{r}) = \sum_i \frac{1}{(2\pi\sigma_r^2)^{3/2}} \exp\left[-\frac{(\mathbf{r} - \mathbf{r}_i)^2}{2\sigma_r^2}\right], \qquad (5)$$

$$\rho(\mathbf{p}) = \sum_i \frac{1}{(2\pi\sigma_p^2)^{3/2}} \exp\left[-\frac{(\mathbf{p} - \mathbf{p}_i)^2}{2\sigma_p^2}\right]. \qquad (6)$$

In the IQMD model, the nucleons in a system move under a self-consistently generated mean field, and the time evolution of $\mathbf{r}_i$ and $\mathbf{p}_i$ is governed by Hamiltonian equations of motion

$$\dot{\mathbf{r}}_i = \frac{\partial H}{\partial \mathbf{p}_i}, \dot{\mathbf{p}}_i = -\frac{\partial H}{\partial \mathbf{r}_i}. \qquad (7)$$

The Hamiltonian H which consists of both kinetic energy and effective interaction potential energy is given by

$$H = \sum_i \frac{\mathbf{p}_i^2}{2\mu} + U^{dd} + U^{yuk} + U^{sym} + U^{coul}, \qquad (8)$$

where μ is the mass of a nucleon, U^{dd} the density-dependent (Skyrme) potential, U^{yuk} the Yukawa potential, U^{sym} the symmetry energy term and U^{coul} the coulomb energy, they have the following forms

$$U^{dd} = \alpha\left(\frac{\rho}{\rho_0}\right) + \beta\left(\frac{\rho}{\rho_0}\right)^\gamma, \qquad (9)$$

$$U^{yuk} = \frac{v_y}{2} \sum_{i,j\neq i} \frac{1}{r_{ij}} \exp(\sigma_r^2 m^2)$$
$$\cdot\left[\exp(mr_{ij})erfc(m\sigma_r - \frac{r_{ij}}{2\sigma_r})\right.$$
$$\left. - \exp(mr_{ij})erfc(m\sigma_r + \frac{r_{ij}}{2\sigma_r})\right], \qquad (10)$$

TABLE I: The parameters adopted in present work.

$\alpha(GeV)^a$	$\beta(GeV)$	γ	$\rho_0(fm^{-3})$	$v_y(GeV)$	m	$C_{sym}(GeV)$
-0.356	0.303	1.17	0.16	-0.0024	0.83	0.032

^{a}Here α, β and γ values correspond to soft potential

$$U^{sym} = \frac{C_{sym}}{2\rho_0} \sum_{i,j \neq i} \tau_{iz}\tau_{jz} \frac{1}{(4\pi\sigma_r^2)^{3/2}} \exp\left[-\frac{(r_i - r_j)^2}{4\sigma_r^2} \right],$$
(11)

$$U^{coul} = \frac{e^2}{4} \sum_{i,j \neq i} \frac{1}{r_{ij}}(1 + \tau_{iz})(1 - \tau_{jz})erfc(\frac{r_{ij}}{4\sigma_r^2}). \quad (12)$$

Here $r_{ij} = |r_i - r_j|$ is the relative distance of nucleon i and j, τ_{iz} the zth component of the isospin degree of freedom for the ith nucleon, which is equal to 1 and -1 for proton and neutron, respectively, C_{sym} is the symmetry potential coefficient. The parameters in this work are listed in Table I.

The nucleon-nucleon (NN) cross section used in present IQMD model is experimental parametrization [33] (σ_{exp}) which is isospin dependent, the neutron and proton are distinguished from each other in the initialization of projectile and target nuclei, and the Pauli blocking of proton and neutron in IQMD is also treated separately as well [30]. In our work, the fragment (or cluster) is recognized by a simple coalescence model: i.e., nucleons are considered to be part of a cluster in every moment at least another nucleon is closer than $r_{min} \leq 3.5 fm$ in the coordinate space.

B. Sequential decay model: GEMINI

The primary fragments from IQMD are excited, in order to compare with the experimental observable, the GEMINI sequential decay model [34, 35] has been used as an afterburner to follow the de-excitation of these excited fragments. In GEMINI all possible sequential decay channels from light particle evaporations to symmetry fission are considered. The sequential decay is traced by a Monte-Carlo technique until the excitation energy of the excited fragment is exhausted. In IQMD calculation the angular momentum is not considered, hence the secondary decay treatment in the GEMINI does not include the angular momentum calculation. In other word, for each sequential decay tracing, the initial angular momentum is set to zero in GEMINI, and in present work all asymmetric divisions are considered. More details about GEMINI can be found in Refs. [33, 35]. IQMD calculation is on the basis of event-by-event, so the secondary decay by GEMINI is managed event-by-event too. Each fragment calculated in one IQMD event will put into the GEMINI to let them decay. The excitation energy of the primary fragments is calculated by following equation

$$E^* = E_{inc}^{c.m.} - \sum_{mult} E_{kin}^{c.m.} - Q, \quad (13)$$

where $E_{inc}^{c.m.}$ is the incident kinetic energy in Center of Mass (c.m.) system and $E_{kin}^{c.m.}$ is the fragment kinetic energy in c.m. system. The summer is made over all the fragments of each event, the Q-value is calculated by the mass excess in each event, then the excitation energy per nucleon E^*/A was uniformly distributed in all nucleons.

In this paper all asymmetric divisions was considered(including both intermediate mass fragment(IMF) and fission decay) in the GEMINI secondary decay calculation, after GEMINI calculation, the final products were collected inclusively again.

III. ISOCALING PROPERTIES AND THE DYNAMICAL AND SECONDARY DECAY EFFECTS

Calculations were carried out in two similar central collisions with impact parameter $b = 1$ of ^{40}Ca + ^{40}Ca and ^{48}Ca + ^{48}Ca at incident energy $E/A = 35$ MeV. In order to investigate the isoscaling dynamical effect, at different reaction time fragments were recorded until 400 fm/c, about 50 thousands events are simulated.

Equation (1) can be expressed as a function of only atomic number Z when the neutron number N is fixed

$$R_{21}(Z) = Y_2(N,Z)/Y_1(N,Z) = C' \exp(\alpha N), \quad (14)$$

or a function of neutron number N when the atomic number Z is fixed

$$R_{21}(Z) = Y_2(N,Z)/Y_1(N,Z) = C'' \exp(\beta Z). \quad (15)$$

Isoscaling of hot fragments was observed at different reaction time from $t = 160$fm/c to 400fm/c, fragments mentioned here include all of the fragments formed in that moment. In fig. 1 two examples of R_{21} were shown for the fragments at reaction time $t = 240$ fm/c as a function of atomic number Z and neutron number N, respectively. R_{21} shows perfect linear dependence as a function of N or Z from light fragments to heavy fragments. Here only reaction time $t = 240$ fm/c are plotted as one sample, the results at other reaction times have similar behaviors. Here we adopt the widely used convention to denote with the index "2" the more neutron-rich system ^{48}Ca + ^{48}Ca and with the index "1" the more neutron-poor system ^{40}Ca + ^{40}Ca.

From Equation (14) and (15) the isoscaling slope parameters α and β can be directly extracted, in this paper only parameter α is analyzed, since parameter β has similar trend with α except that β value is negative. In fig. 2(a), parameter α as a function of the fragment charge number Z was printed at several reaction time, one can
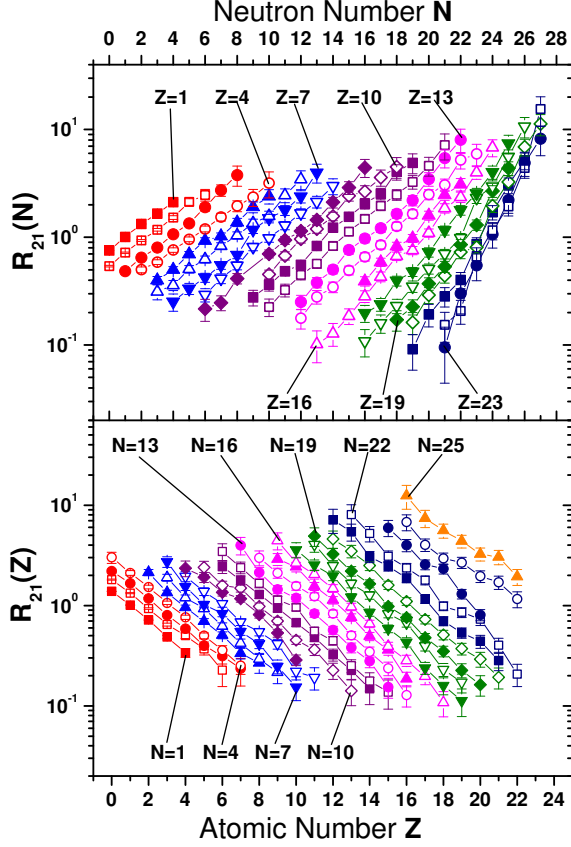
FIG. 1: Isotopic yield ratios (upper panel) and Isotonic yields ratios (bottom panel) of primary fragments at reaction time $t = 240 fm/c$ between $^{48}Ca + ^{48}Ca$ and $^{40}Ca + ^{40}Ca$ in the IQMD model with impact parameter $b = 1fm$ and incident energy $E_{inc} = 35 MeV/A$, different symbols from left to right represent the isotope sequence from $Z = 1$ to $Z = 23$ (upper panel) and isotone sequence from $N = 1$ to $Z = 25$ (bottom panel), in this figure the error bar comes from only statistics

find that for the light and intermediate mass fragments, such as $Z \leq 15$, α value does not change too much with the fragment charge number Z, but for the heavy fragments, α shows different behavior from the light ones, it increases with the fragments charge number Z. One can also find that the isoscaling parameter α presents very small decrease when the reaction time becomes longer, at $t = 140$ fm/c α lies on the top, $t = 400$ fm/c α locates at the bottom. However, this is suitable only for the light products, and it is opposite for the heavy products though the dynamical effect is not clear.

From a practical point of view, the isotopic distributions of a given Z fragment $Y(N)|_Z$ can be approximately described by Gaussian function. Using the general notation for the isotopic distribution in a given Z, $Y(N)|_Z$
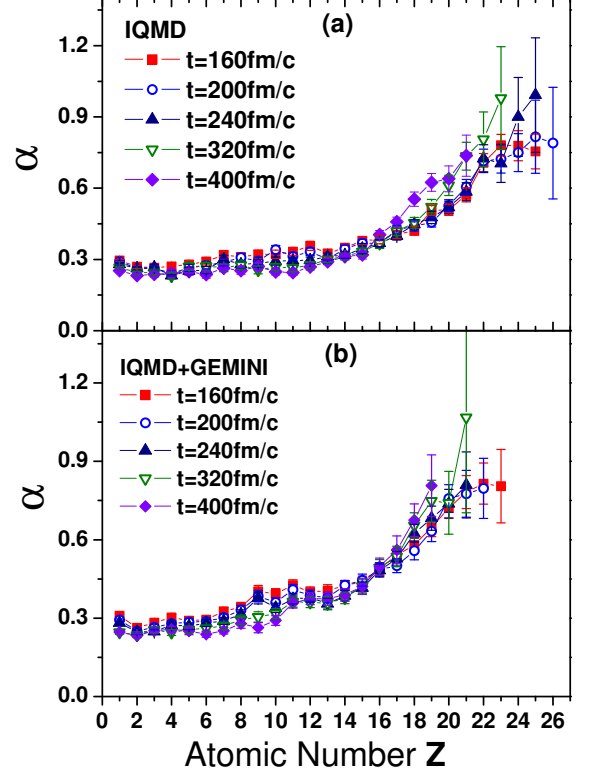

FIG. 2: Isoscaling parameter α as a function of the fragment atomic number Z, different symbols represent α at different reaction time, panel (a): IQMD calculation results; panel (b): IQMD+GEMINI calculation results.

can be described by a single Gaussian function as

$$Y(N)|_Z = C \exp\left[-\frac{(N - \langle N_Z \rangle)^2}{2\sigma_Z^2} \right], \qquad (16)$$

where $\langle N_Z \rangle$ is the centroid of isotopic distributions, and σ_Z describes the variance of distributions for each element of charge Z, then for a fixed element of charge Z the ratio of isotopic yields writes

$$
\begin{aligned}
R_{21}(N) &= \frac{Y_2(N)|_Z}{Y_1(N)|_Z} \\
&= C' \exp\left[N\left(\frac{\langle N_2 \rangle}{2\sigma_2^2} - \frac{\langle N_1 \rangle}{2\sigma_1^2} \right) \right] \\
&\quad \cdot \exp\left[N^2\left(\frac{1}{2\sigma_1^2} - \frac{1}{2\sigma_2^2} \right) \right] \qquad (17)
\end{aligned}
$$

where $\langle N_1 \rangle$ and $\langle N_2 \rangle$ are the centroids for isotopic distributions of neutron-poor system ^{40}Ca + ^{40}Ca and neutron-rich system ^{48}Ca + ^{48}Ca, σ_1 and σ_2 describe the variance of distributions in these two systems, respectively, here the fragment charge number Z is fixed.
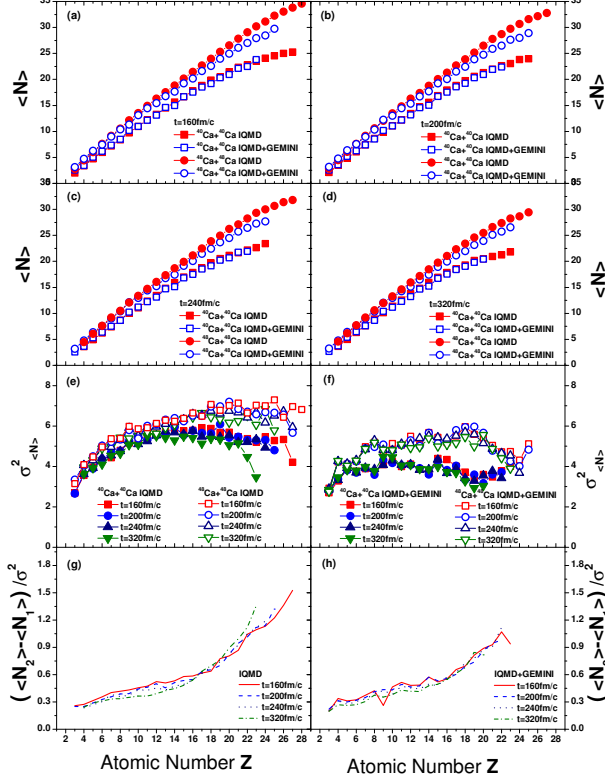
FIG. 3: The centroid $\langle N \rangle$ and width σ^2 of Gaussian isotopic distribution as a function of the atomic number Z at different reaction times for the primary products in IQMD calculation and final products in IQMD+GEMINI calculation. Panels (a) -(f): centroid $\langle N \rangle$ as a function of Z at different evolution time in two systems; panel (e) and (f): σ^2 as a function of Z, (g) and (h): calculated $(\langle N_2 \rangle - \langle N_1 \rangle)/\sigma^2$ from upper panels.

From equation (17) one can notice that if the second order N^2 in the exponential function can be neglected, $\ln(R_{21}(N))$ is linear dependence on neutron number N for a fixed element with charge number Z, and α value can be expressed as $\langle N_2 \rangle / 2\sigma_2^2 - \langle N_1 \rangle / 2\sigma_1^2$. Fig. 3 shows the centroid $\langle N \rangle$ and width σ^2 of Gaussian isotopic distributions as a function of atomic number Z of the emitted products at different reaction time (panel (a) - (f)) before and after secondary decay, panel (a) to (d), the difference of $\langle N_2 \rangle$ in $^{48}\text{Ca} + ^{48}\text{Ca}$ system and $\langle N_1 \rangle$ in $^{40}\text{Ca} + ^{40}\text{Ca}$ system increases when atomic number Z of the emitted products becomes large, in panel (e) and (f) of fig. 3, the width σ^2 of isotopic distributions does not same in two similar reactions too, it increases with the increasing of fragment atomic number Z, reaches saturation at some point. In fig. 3(g), $(\langle N_2 \rangle - \langle N_1 \rangle)/2\sigma^2$ is plotted as a function of Z, here $\sigma^2 = (\sigma_1^2 + \sigma_2^2)/2$ was adopted, it redisplays the α behavior in fig. 2, its value raises from the light fragments to heavy fragment, especially in the heavy fragment part, it raises sharply. It decreases in
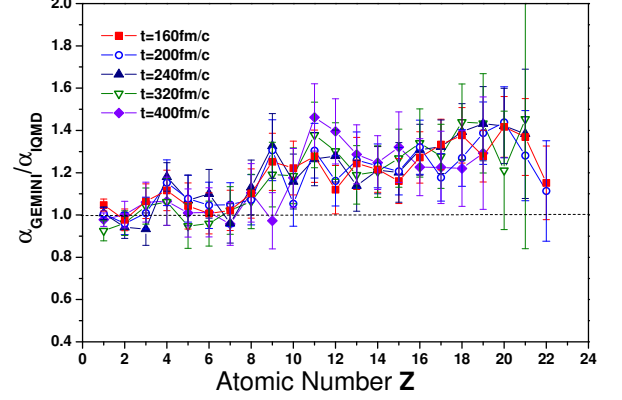

FIG. 4: The ratio of isoscaling parameters α between final and primary products.

the region of light and intermediate mass fragments with increasing of the reaction time, but opposite trend in the region of heavy fragments. This reveals that neglecting the second order in equation (17) is reasonable in most cases.

The secondary decay effect on isoscaling was investigated by the GEMINI code [34, 35] calculation. In this code, the fragment charge number Z, fragment mass A and the excitation energy of the fragment is the only input for the GEMINI code. In each event simulated by the IQMD, each fragment with charge number great than 7 will consider sequential decay, the reason why the sequential decay for fragment charge number great than 7 will be discussed later. Since in the IQMD model, the angular momentum conservation was not taken into account, the angular momentum of each fragment is not calculated, the angular momentum of the hot product was set to zero as input to GEMINI. Isoscaling behavior of final products after the secondary decay are also observed. α parameters were extracted with equation (14) as a function of the fragment atomic number Z and shown in fig. 2(b), one can find that the dynamical effect due to different reaction times is still clear for the light fragments, here the different reaction time refers to the time the fragments were collected in IQMD calculation and the GEMINI calculation starts. The secondary decay effect, however, does not depend on the switching time of dynamical IQMD to GEMINI code for the final products after secondary decay. α basically keeps not change for the light fragments even though the secondary decay, but increases for the heavy products with the increasing of the products atomic number Z. In order to quantitatively compare the secondary decay effect on isoscaling parameters, the ratio between α_{GEMINI} and α_{IQMD} was plotted in fig. 3, one can see that the ratios fluctuate around 1.0 for the light fragment with atomic number $Z \leq 8$ and ~ 1.2 for the products charge number
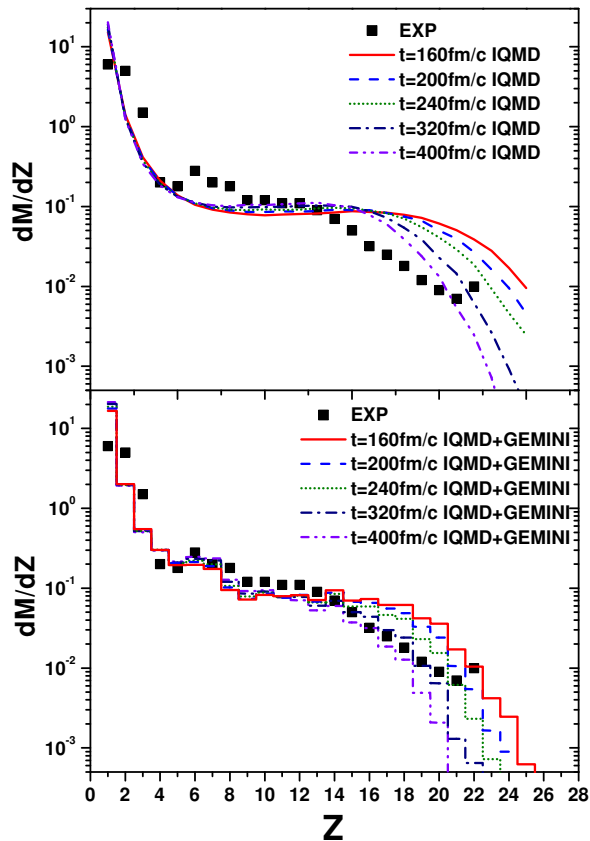
FIG. 5: Comparison of charge distribution between the experimental data (solid square) [36] and IQMD calculation (line) or IQMD + GEMINI (histogram) calculation at different reaction time.

$Z > 8$.

The light fragments include both the primary products which do not experience sequential decay and the secondary decayed products from the heavy primary products, however, this mixture of light fragments do not affect the isoscaling phenomenon. It reveals that the light primary fragments have same N/Z as the final products decayed from the heavy primary products, they have achieved local equilibration or stable isotopic distribution on the isospin degree of freedom, so N/Z of light fragments is not affected by the secondary decay process. It is a good observable to study the primary products isospin information, which have been confirmed by many experiment and theoretical researches[8, 9, 11, 12, 16, 17, 18, 21, 22, 23].

In IQMD and GEMINI calculation, the fragment charge distributions of IQMD and GEMINI with the experimental data [36] have been compared in fig. 5. The top panel is the comparison of fragment charge distribution between experimental data [36] and the IQMD calculation, it looks that heavier products have been overes-

TABLE II: Average excitation energies per nucleon and the temperature calculated at different reaction times for two similar reaction systems ^{40}Ca + ^{40}Ca and ^{48}Ca + ^{48}Ca with incident energy $E_{inc} = 35$ MeV/A and impact parameter $b = 1$fm.

t	$160 fm/c$	$200 fm/c$	$240 fm/c$	$320 fm/c$	$400 fm/c$
$\langle E^*/A \rangle^a$	4.812	4.524	4.274	3.871	3.584
T^a	6.937	6.726	6.537	6.222	5.987
$\langle E^*/A \rangle^b$	5.511	5.214	4.943	4.496	4.179
T^b	7.423	7.221	7.030	6.705	6.464
$\langle T \rangle^c$	7.180	6.974	6.784	6.463	6.226

^{a}average excitation energy per nucleon and temperature in collision ^{40}Ca + ^{40}Ca

^{b}average excitation energy per nucleon and temperature in collision ^{48}Ca + ^{48}Ca

^{c}average temperature $\langle T \rangle$ of ^{40}Ca + ^{40}Ca and ^{48}Ca + ^{48}Ca reactions, $\langle T \rangle = (T^a + T^b)/2$

timated, but the intermediate mass fragments were underestimated in calculations. This problem was nicely solved after the secondary decay with the GEMINI code was taken into account (see bottom panel of fig. 5), especially when the switching time of IQMD fragments equals to 240 fm/c or 320 fm/c. The best description of the final charge distribution of products after GEMINI calculation lies on the bump of $Z \approx 6$, this bump emerges only when secondary decay of the primary fragments with $Z \geq 8$ are taken into account and while the secondary decay of primary fragments with $Z < 8$ are not considered. This may be the condition that the isoscaling parameters α is not affected by the secondary decay.

IV. DENSITY DEPENDENCE OF THE SYMMETRY ENERGY COEFFICIENT

The excitation energy per nucleon (E^*/A) was calculated from equation (13), E^*/A distributions have the Gaussian shape, from which the average excitation energy per nucleon ($\langle E^*/A \rangle$) can be obtained. In table II list the average excitation energy per nucleon at different reaction times for both similar reaction systems, the temperature is extracted from equation $E^*/A = a \cdot T^2$, $a = 1/10$ was adopted. The excitation energy of the system has high values at early reaction time and it decreases with the evolution of the system. At different reaction time the temperature extracted from two reaction systems ^{40}Ca + ^{40}Ca and ^{48}Ca + ^{48}Ca has approximately same values, so the average temperature in this two reactions are calculated simply to use as a parameter in following calculation, which are listed in table II too.

Using equation (2), from the extracted values of α, average temperature $\langle T \rangle$ of the two systems, and the $\langle Z/A \rangle$ of the fragments in two reaction systems, symmetry energy coefficient C_{sym} in the EOS can be derived. In present calculation, the $\langle Z/A \rangle$ was fitted from its Z/A distributions of the primary and final products respec-
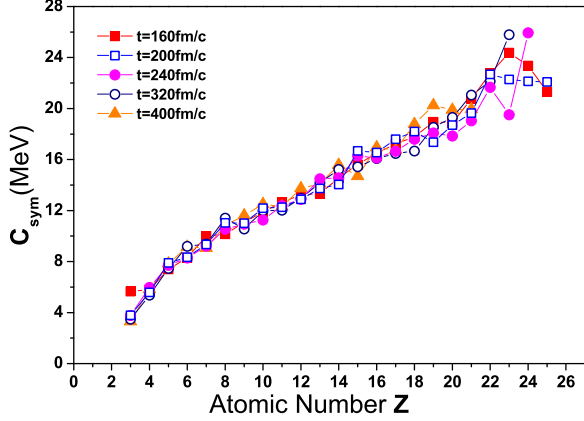
FIG. 6: Symmetry energy coefficients C_{sym} as a function of the primary products atomic number Z from IQMD calculation.
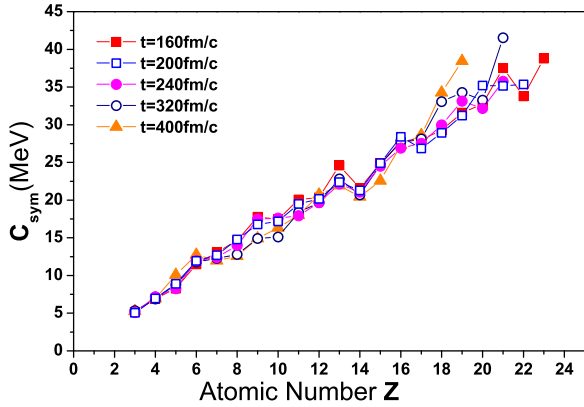

FIG. 7: Symmetry energy coefficients C_{sym} as a function of the final products atomic number Z from IQMD+GEMINI calculation.

tively, which are Gaussian distribution too and can get the average Z/A in two reactions $\langle Z_1/A_1 \rangle$ and $\langle Z_2/A_2 \rangle$. The derived symmetry energy coefficient C_{sym} was plotted as a function of the atomic number Z of products for primary products in fig. 6 and final products in fig. 7.

One can find that the symmetry energy coefficient C_{sym} for different products with different atomic number Z is not a constant in the present calculation, it increases with the increasing of the products charge number Z, and the dynamics effect is almost vanished. To understand why the symmetry energy coefficient C_{sym} was not a constant for different products, the densities of the products with different atomic number Z in IQMD simulation were extracted. In the IQMD frame, the fragments are treated as cluster by simple coalescence model, the central densi-
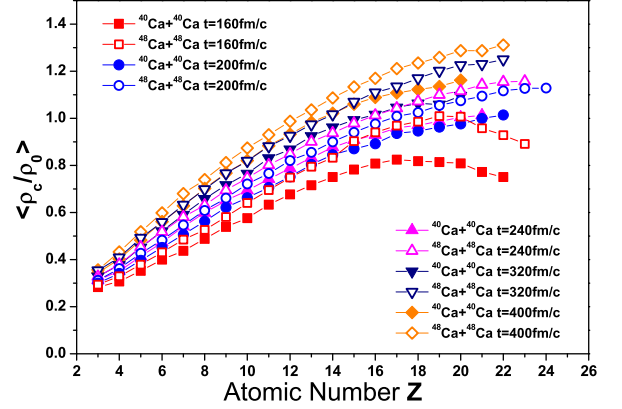

FIG. 8: Average central density $\langle \rho_c/\rho_0 \rangle$ of the clusters in the rest frame of cluster as a function of the cluster proton number Z at different times for two reactions.

ties of clusters were calculated by equation (4) with $\vec{r} = 0$ in the cluster coordinate phase space, and sum over all nucleons inside the same cluster. The central density distribution ρ_c/ρ_0 of the clusters is generally Gaussian form and $\langle \rho_c/\rho_0 \rangle$ can be fitted from this Gaussian distribution, here $\rho_0 = 0.16 fm^{-3}$ refers to the normal nuclear matter density. Fig. 8 shows the fitted average central densities as a function of the cluster charge number Z at different reaction times in two reactions ^{40}Ca + ^{40}Ca and ^{48}Ca + ^{48}Ca. The light clusters are always in the very low density region, while the heavy clusters can approach to the saturation density. Remind that the nucleon can be considered to be emitted if its density is lower than a certain low values, eg. $\rho_0/10$ in some transport calculations, the above curve of $\rho(Z)$ support this argument. For reaction system ^{48}Ca + ^{48}Ca, a little higher average central densities $\langle \rho_c/\rho_0 \rangle$ of clusters than those in ^{40}Ca + ^{40}Ca are observed since the cluster with same proton numbers Z formed in reaction system ^{48}Ca + ^{48}Ca has more neutrons than in reaction system ^{40}Ca + ^{40}Ca, which has been verified by the $\langle N \rangle$ distribution from fig. 3. The average central density of clusters in two reaction systems have some divergence, in the later discussions, the average values of $\langle \rho_c/\rho_0 \rangle_{ave} = (\langle \rho_c/\rho_0 \rangle_1 + \langle \rho_c/\rho_0 \rangle_2)/2$ of these two reactions is adopted.

Since both symmetry energy coefficient C_{sym} and the average cluster central density $\langle \rho_c/\rho_0 \rangle_{ave}$ are correlated with the atomic number Z of products, the symmetry energy coefficient C_{sym} can relate with the average central density $\langle \rho_c/\rho_0 \rangle_{ave}$ by eliminating the products atomic number Z. The slight difference of different reaction time information was expressed by adding error bars to the derived C_{sym}. Fig. 10 demonstrates the relationship between symmetry energy coefficient C_{sym} and average central density $\langle \rho_c/\rho_0 \rangle_{ave}$. The density dependence of the symmetry energy term in equation of state (EOS)
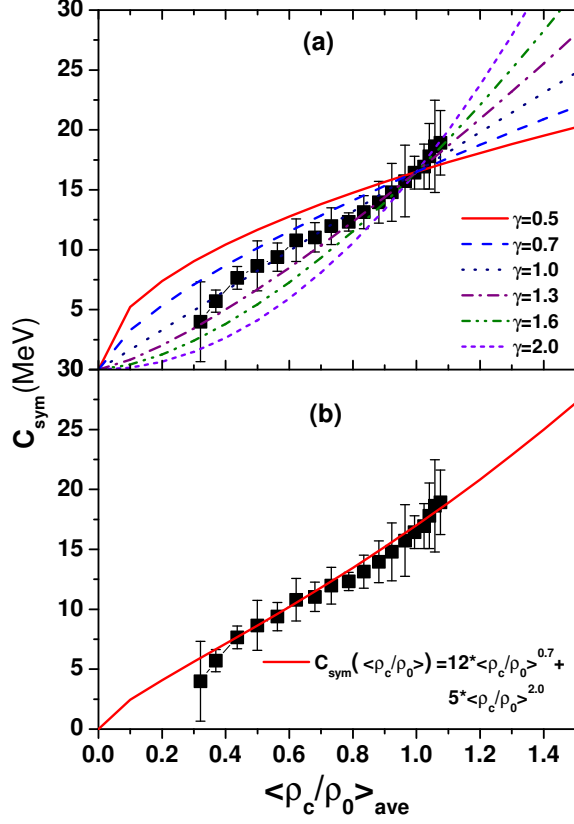
FIG. 9: The relationship between symmetry energy co-efficient C_{sym} and the average central density $\langle \rho_c/\rho_0 \rangle_{ave}$, solid square represents the IQMD calculations, the error bar represents the average over different reaction times. Panel (a): different lines represent the formula (18) fitting with $C_0 = 16.5$ MeV and different parameter γ which are shown in the insert; Panel (b): Combination of two set parameters $C_{sym}(\langle \rho_c/\rho_0 \rangle) = 12 \cdot \langle \rho_c/\rho_0 \rangle^{0.7} + 5 \cdot \langle \rho_c/\rho_0 \rangle^{2.0}$

FIG. 10: The relationship between symmetry energy coefficient C_{sym} and the average central density $\langle \rho_c/\rho_0 \rangle_{ave}$, solid square represents the IQMD+GEMINI calculations and the error bar represents the average over different reaction times. Panel (a): different lines represent the formula (18) fitting with $C_0 = 26 MeV$ and different parameter γ which are displayed in the insert; Panel (b): Combination of two set parameters $C_{sym}(\langle \rho_c/\rho_0 \rangle) = 12 \cdot \langle \rho_c/\rho_0 \rangle^{0.7} + 5 \cdot \langle \rho_c/\rho_0 \rangle^{2.0}$

was generally expressed by following equation

$$C_{sym}(\rho) = C_0 \left(\frac{\rho}{\rho_0} \right)^{\gamma} \tag{18}$$

where γ represents the stiffness of the symmetry energy. Some tests have been done for the determination of the parameter C_0 and γ in fig. 10. In panel (a) a constant C_0 = 16.5 MeV is used but some different values of γ, namely 0.5, 0.7, 1.0, 1.3, 1.6 and 2.0 were taken, respectively, to fit the IQMD calculation results, one can find that $\gamma = 1.0$ seems to be the best fit to the IQMD calculation than other γ values in the low $\langle \rho_c/\rho_0 \rangle_{ave} < 1.0$ region, but in $\langle \rho_c/\rho_0 \rangle_{ave} > 1.0$ region divergence arises between the IQMD calculation and the fitting, it seems that in high $\langle \rho_c/\rho_0 \rangle_{ave} > 1.0$ part, C_{sym} raises sharply which corresponds to a γ value great than 1.0. In panel (b) the line is two different parameters combination of equation (18), $C_{sym}(\langle \rho_c/\rho_0 \rangle_{ave}) = 12 \cdot \langle \rho_c/\rho_0 \rangle_{ave}^{0.7} + 5 \cdot \langle \rho_c/\rho_0 \rangle_{ave}^{2.0}$, in the low density region $\langle \rho_c/\rho_0 \rangle_{ave} \leq 1.0$, has the
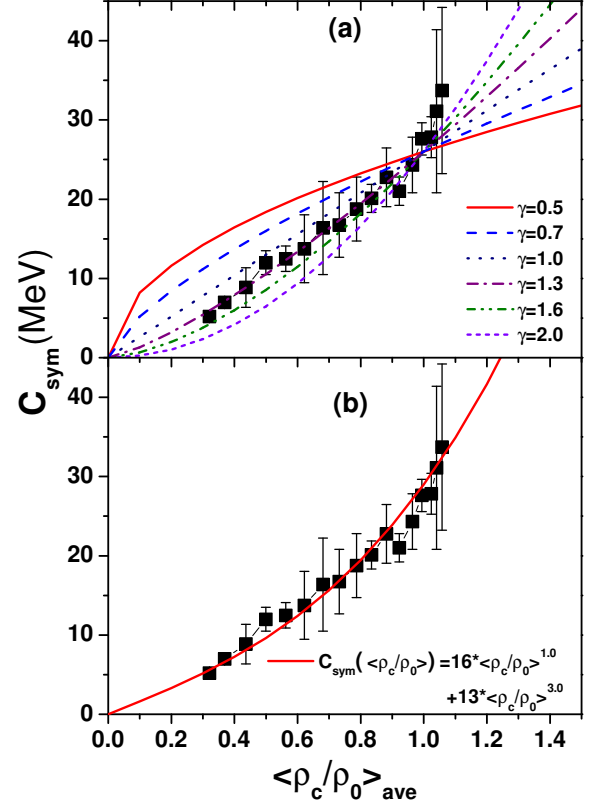
similar shape with the above mentioned simple form $C_{sym}(\langle \rho_c/\rho_0 \rangle_{ave}) = 16.5 \cdot \langle \rho_c/\rho_0 \rangle_{ave}^{1.0}$, but better behavior than the simple form with only $\gamma = 1.0$. This demonstrates that in the whole density region, the symmetry energy coefficient C_{sym} as a function of the nuclear density can not be well described by only one simple equation (18) in the present model calculation, but expressed by the various contribution from two sets of EOS (18). In present calculation of IQMD, the simple equation such as $C_{sym}(\langle \rho_c/\rho_0 \rangle_{ave}) = 12 \cdot \langle \rho_c/\rho_0 \rangle_{ave}^{0.7} + 5 \cdot \langle \rho_c/\rho_0 \rangle_{ave}^{2.0}$ is a good approximation for the C_{sym} and $\langle \rho_c/\rho_0 \rangle_{ave}$.

Fig. 10 plots the relationship between C_{sym} and $\langle \rho_c/\rho_0 \rangle_{ave}$ after considering the secondary decay. Panel (a) shows the IQMD + GEMINI calculation C_{sym} as a function of average central density $\langle \rho_c/\rho_0 \rangle_{ave}$, several fits with a constant $C_0 = 26 MeV$ and different $\gamma = 0.5$, 0.7, 1.0, 1.3, 1.6, 2.0 of equation (18) have been made, in which $\gamma = 1.3$ looks to fit the calculation best in

the density region $\langle \rho_c/\rho_0 \rangle_{ave} \leq 1.0$, equation (18) with $\gamma > 1.3$ works better in the higher density part. Equation $C_{sym}(\langle \rho_c/\rho_0 \rangle_{ave}) = 16 \cdot \langle \rho_c/\rho_0 \rangle_{ave}^{1.0} + 13 \cdot \langle \rho_c/\rho_0 \rangle_{ave}^{3.0}$ was also adopted in panel (b) to fit the calculation in fig. 10, it can give a good coincidence between the calculation of IQMD+GEMINI and the equation (18) fitting.

No matter a simple form of equation (18) was used, or combination of different set parameters of equation (18) was used, different parameter C_0 was got for the primary products in IQMD calculation and final products in IQMD+GEMINI calculation. In the simple form of equation (18) for fitting IQMD calculation, $C_0 = 16.5$ MeV was got, while fitting IQMD + GEMINI calculation $C_0 = 26$ MeV was got. The different symmetry energy coefficients C_0 extracted from primary and final products indicate that the secondary decay affects the extraction of symmetry energy coefficient C_0.

From the fits to the IQMD and IQMD+GEMINI calculations, the subnormal density region can be described better by a soft symmetry energy with $\gamma < 1.0$, the supernormal density region can be described better by a stiff symmetry energy with $\gamma > 1.0$. This demonstrates that in the subnormal and supernormal density regions, the symmetry energy shows different behavior, the best description of the relationship between symmetry energy coefficient C_{sym} and the nuclear density $\langle \rho/\rho_0 \rangle$ in full density region should be combination of equation (18) with at least one "soft" symmetry term with $\gamma \leq 1.0$ and one "stiff" symmetry term with $\gamma > 1.0$ [28].

V.   CONCLUSIONS

In summary, we applied the Isospin dependent Quantum Molecular Dynamics (IQMD) model to investigate the isoscaling behavior in dynamical and statistical sequential decay processes of both reactions ^{40}Ca + ^{40}Ca and ^{48}Ca + ^{48}Ca at $b = 1$ fm. The calculation illustrates that both primary and final isotopic yields show the isoscaling behavior.

The isoscaling parameter α have similar values for the light and intermediate mass fragments, but it increases much with the fragments become heavy. α shows some dynamical effect, i.e. it drops slowly with the increasing of reaction times. The light final products which do not experience secondary decay itself are not affected by the secondary decay, but the isoscaling parameter α of the heavy products which experience secondary decay process increase in comparison with the primary products.

Average central density of the clusters is calculated in the IQMD calculation, it raises with the increasing of charge number of clusters until the saturation density close to the normal nuclear matter density $\rho_0 = 0.16$ fm^{-3}. From the equation (18), the density dependence of the symmetry energy coefficient C_{sym} can be extracted from the IQMD and IQMD+GEMINI calculation. The results show that even though the density dependence of the symmetry energy coefficient C_{sym} can be approximately described by a $\gamma \sim 1.0$, it is more reasonable to express this dependence by the combination of "soft" and "stiff" symmetry energy term. From equation (18), the extracted symmetry energy coefficient C_{sym} is also affected by the secondary decay process, i.e. it leads to different values of C_0 and γ from the initial values of IQMD.

[1] *Isospin Physics in Heavy Ion Collisions at Intermadiate Energies*, edited by B.-A. Li and W. Schroeder(Nova Science, New York, 2001)
[2] M. Di. Toro *et al*, Prog. Nucl. Nucl. Phys. **42**, 125 (1999), *and references therein*
[3] B.A. Li, C.M. Ko and W. Bauer, Int. J. Mod. Phys. E **7**, 147 (1998), *and references therein*
[4] Y. G. Ma *et al*, Phys. Rev. C **60**, 024607 (1999)
[5] H. Müller and B. D. Serot, Phys. Rev. C **52**, 2072 (1995)
[6] I. Bombaci, T. S. Kuo and U. Lombardo, Phys. Rep. **242**, 165 (1994)
[7] S. Das Gupta, A. Z. Mekjian and M. B. Tsang, Adv. Nucl. Phys. **26**, 91 (2001)
[8] H. S. Xu *et al*,Phys. Rev. Lett. **85**, 716 (2000)
[9] M.B. Tsang *et al*, Phys. Rev. C **64**, 041603(R) (2001)
[10] M.B. Tsang *et al*, Phys. Rev. Lett. **86**, 5023 (2001)
[11] M.B. Tsang *et al*, Phys. Rev. C. **64**, 054615 (2001)
[12] J. Brzychczyk *et al*, Phys. Rev. C **47**, 1553 (1993)

[13] V. Volkov, Phys. Rep. **44**, 93 (1978)
[14] M. Veselsky, G.A. Souliotis and M. Jandel, Phys. Rev. C **69**, 044607 (2004)
[15] G.A. Souliotis *et al*, Phys. Rev. C **68**, 024605 (2003)
[16] A.S.Botvina, O.V. Lozhkin and W. Trautmann, Phys. Rev. C **65**, 044610 (2002)
[17] E. Geraci *et al*, Nucl Phys. A **732**, 173 (2004)
[18] D.V.Shetty *et al*, Phys. Rev. C **70**, 011601(R) (2004)
[19] K. Wang, Y. G. Ma, Y. B. Wei, X. Z. Cai, J. G. Chen, D. Q. Fang,W. Guo, G. L. Ma,W. Q. Shen,W. D. Tian, C. Zhong, and X. F. Zhou, Chin. Phys. Lett. 22, 53 (2005)
[20] Y. G. Ma, K. Wang, X. Z. Cai, J. G. Chen, J. H. Chen, D. Q. Fang, W. Guo, C. W. Ma, G. L. Ma, W. Q. Shen, Q. M. Su, W. D. Tian, Y. B. Wei, T. Z. Yan, C. Zhong, X. F. Zhou, and J. X. Zuo, Phys. Rev. C **72** 064603 (2005)
[21] Y. G.Ma, K. Wang, Y. B.Wei, G. L.Ma, X. Z. Cai, J. G. Chen, D. Q. Fang, W. Guo, W. Q. Shen, W. D. Tian, and C. Zhong, Phys. Rev. C 69, 064610 (2004).

[22] A. Ono, P. Danielewicz, W. A. Friedman, W. G. Lynch, and M. B. Tsang, Phys. Rev. C **68**, 051601(R) (2003)

[23] W. D. Tian, Y. G. Ma, X. Z. Cai, J. G. Chen, J. H. Chen, D. Q. Fang, W. Guo, C.W. Ma, G. L.Ma, W. Q. Shen, K.Wang, Y. B.Wei, T. Z. Yan, C. Zhong, and J. X. Zuo, Chin. Phys. Lett. 22, 306 (2005).

[24] Ad. R. Raduta, Eur. Phys. J. A **24**, 85 (2005)

[25] J. M. Lattimer and M. Prakash, Phys. Rep. **333**, 121 (2000)

[26] W. D. Myers and W.J. Swiatecki, Nucl. Phys. A **81**, 1 (1966)

[27] A. Le Fèvre *et al*, Phys. Rev. Lett. **94**, 162701 (2005)

[28] Lie-Wen Chen, Che Ming Ko and Bao-An Li, Phys. Rev. Lett. **94**, 032701 (2005)

[29] J. Aichelin *et al*, Phys. Rev. C **37**, 2451 (1988); J. Aichelin, Phys. Rep. **202** 233 (1991)

[30] Chen Liewen, Zhang Fengshou and Jin Genming, Phys. Rev. C **58**, 2283 (1998)

[31] A. Ono, H. Horiuchi, T. Maruyama, A. Ohnishi, Prog. Theo. Phys. **87**, 1185(1992)

[32] M. Papa, T. Maruyama, A. Bonasera, Phys. Rev. C **64**, 024612 (2001)

[33] K. Chen *et al*, Phys. Rev. **166**, 949 (1968)

[34] R.J. Charity *et al*, Nucl. Phys. A **483**, 371 (1988)

[35] R.J. Charity, computer code GEMINI, see http:// wunmr.wustl.edu/pub/gemini

[36] R. Wada *et al*, Phys. Lett. B **422**, 6 (1998)